Supplementary information

Cubic and hexagonal boron nitride phases and phase boundaries

Abhijit Biswas,*[a] Gustavo A. Alvarez,[b] Manoj Tripathi,*[c] Jonghoon Lee,[d] Tymofii S. Pieshkov,[ae] Chenxi Li,[a] Bin Gao,[f] Anand B. Puthirath,[a] Xiang Zhang,[a] Tia Gray,[a] Jacob Elkins,[a] Robert Vajtai,[a] Pengcheng Dai,[f] A. Glen Birdwell,[g] Mahesh R. Neupane,[g] Tony Ivanov,[g] Elias J. Garratt,[g] Bradford B. Pate,[h] Ajit K. Roy,[d] Alan Dalton,*[c] Zhiting Tian,*[b] and Pulickel M. Ajayan*[a]

AFFILIATIONS

[a]Department of Materials Science and Nanoengineering, Rice University, Houston, TX, 77005, USA

[b]Sibley School of Mechanical and Aerospace Engineering, Cornell University, Ithaca, NY 14853, USA

[c]Department of Physics and Astronomy, University of Sussex, Brighton BN1 9RH, United Kingdom

[d]Air Force Research Laboratory, Materials and Manufacturing Directorate, WPAFB, OH, 45431, USA

[e]Applied Physics Graduate Program, Smalley-Curl Institute, Rice University, Houston, TX, 77005, USA

[f]Department of Physics and Astronomy, Rice University, Houston, TX, 77005, USA

[g]DEVCOM Army Research Laboratory, RF Devices and Circuits, Adelphi, Maryland 20783, USA

[h]Naval Research Laboratory, Washington DC 20375, USA

[*]Corresponding Authors: **01abhijit@gmail.com, m.tripathi@sussex.ac.uk, A.B.Dalton@sussex.ac.uk, zhiting@cornell.edu, ajayan@rice.edu**

Keywords: Boron nitride, cubic and hexagonal phases, spark plasma sintering, phase transformation, thermal and mechanical properties

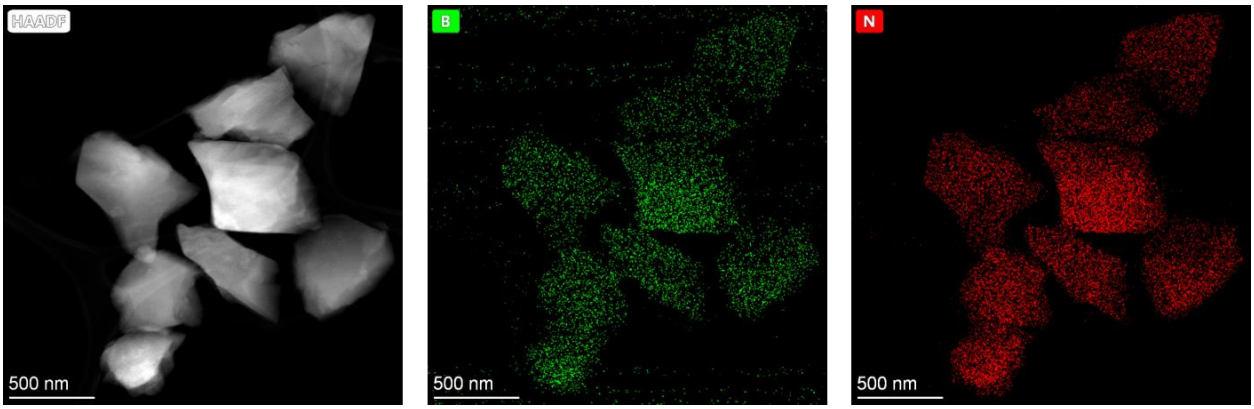

Figure S1. High-angle annular dark-field scanning transmission electron microscopy (HAADF-STEM) image and energy dispersive spectrum (EDS) elemental mappings of boron (B) and nitride (N) in c-BN crystal.

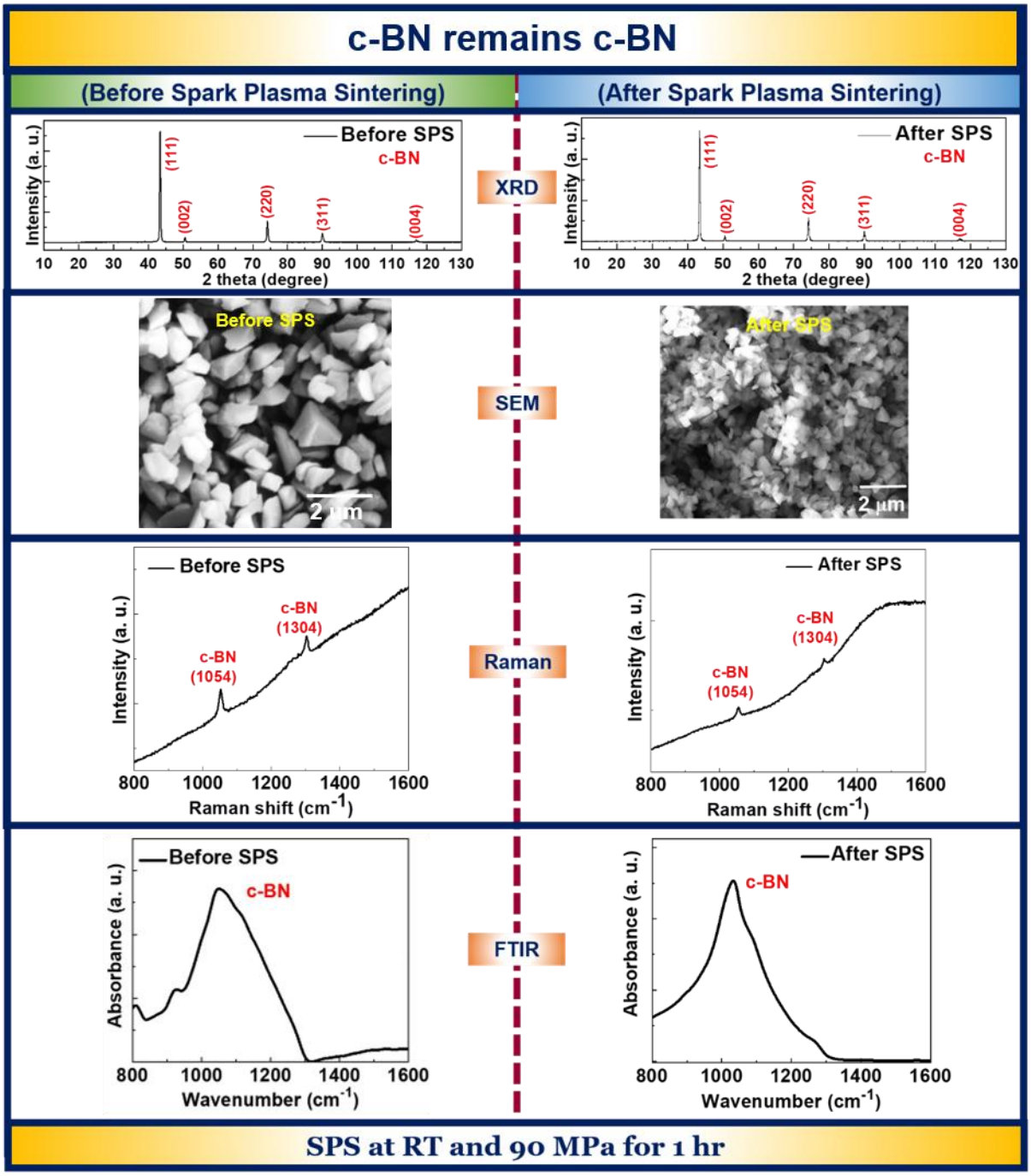

Figure S2. Characterizations of c-BN before (left panel) and after spark plasma sintering (SPS) (right panel). X-ray diffraction (XRD), field-emission scanning electron microscope (FESEM), Raman spectroscopy, and Fourier-transform infrared spectroscopy (FTIR) show that it remains c-BN, after SPS at room temperature and 90 MPa pressure.

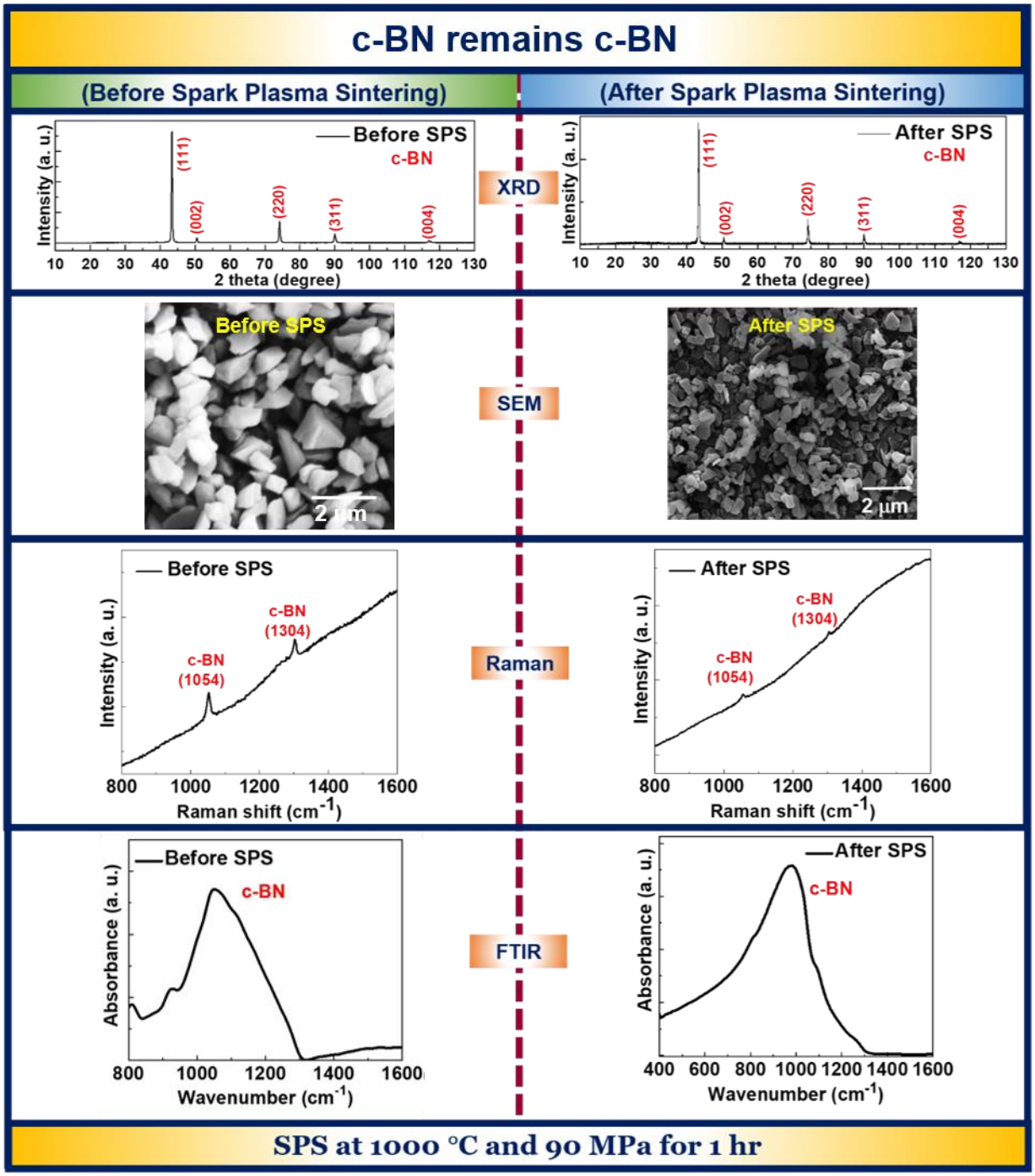

Figure S3. Characterizations of c-BN before (left panel) and after the SPS (right panel). XRD, FESEM, Raman spectroscopy, and FTIR show that it remains c-BN, after SPS at 1000 °C and 90 MPa pressure.

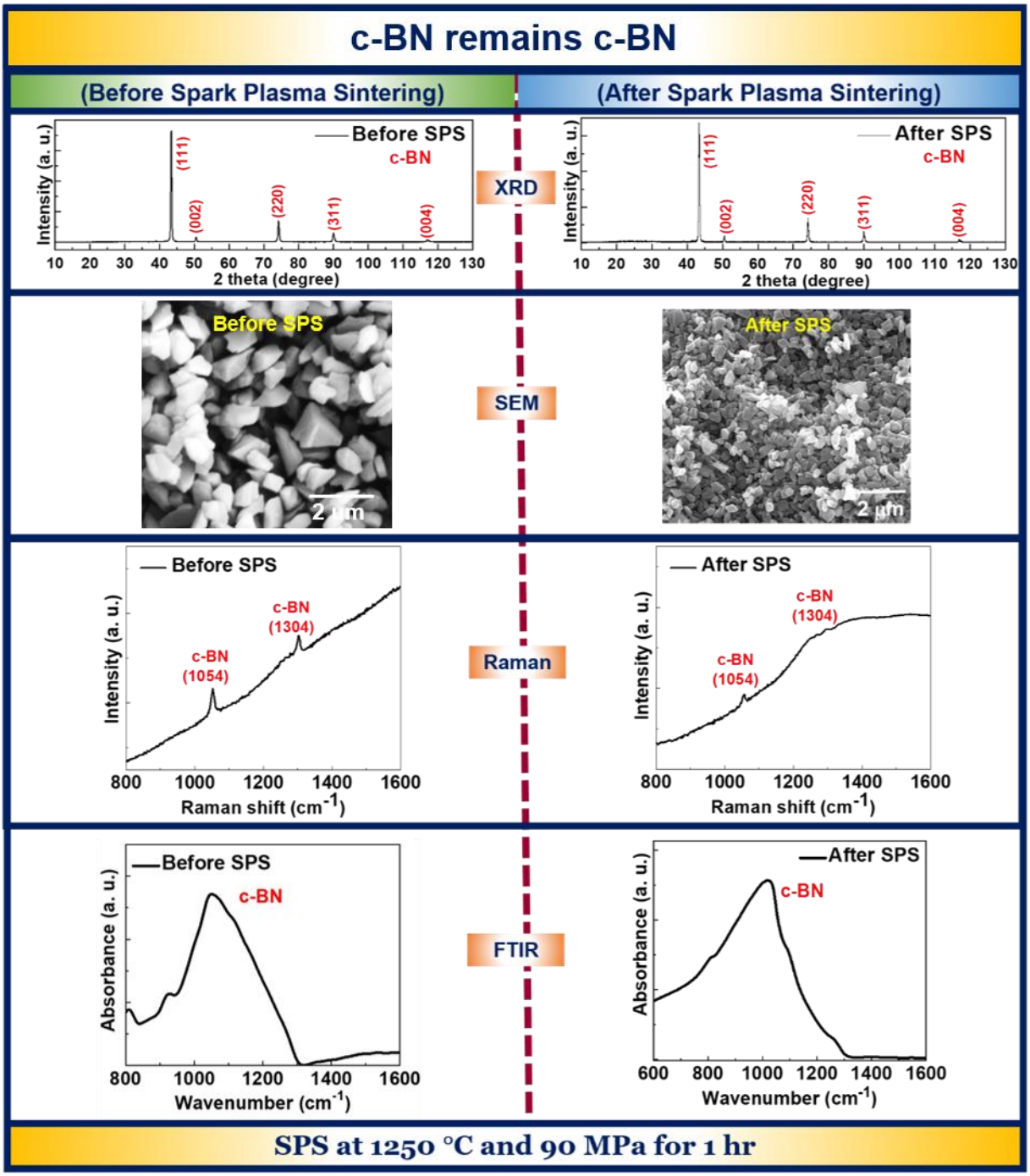

Figure S4. Characterizations of c-BN before (left panel) and after SPS (right panel). XRD, FESEM, Raman spectroscopy, and FTIR shows that it remains c-BN, after SPS at 1250 °C and 90 MPa pressure.

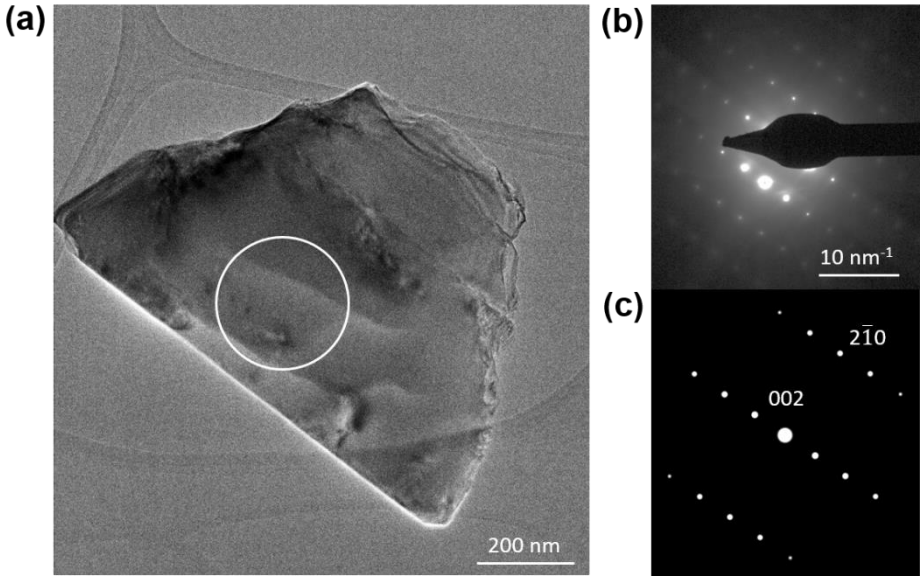

Figure S5. TEM analysis of the BN after the SPS (at 1700 °C, and 90 MPa). (a) Low-magnification TEM image of the h-BN particle displays the overall shape. (b) Selected area electron diffraction (SAED) pattern showing the (100) orientation of the particle. Diffraction image was taken from the circled area from (a). (c) Simulated diffraction patterns of (10−10) h-BN.

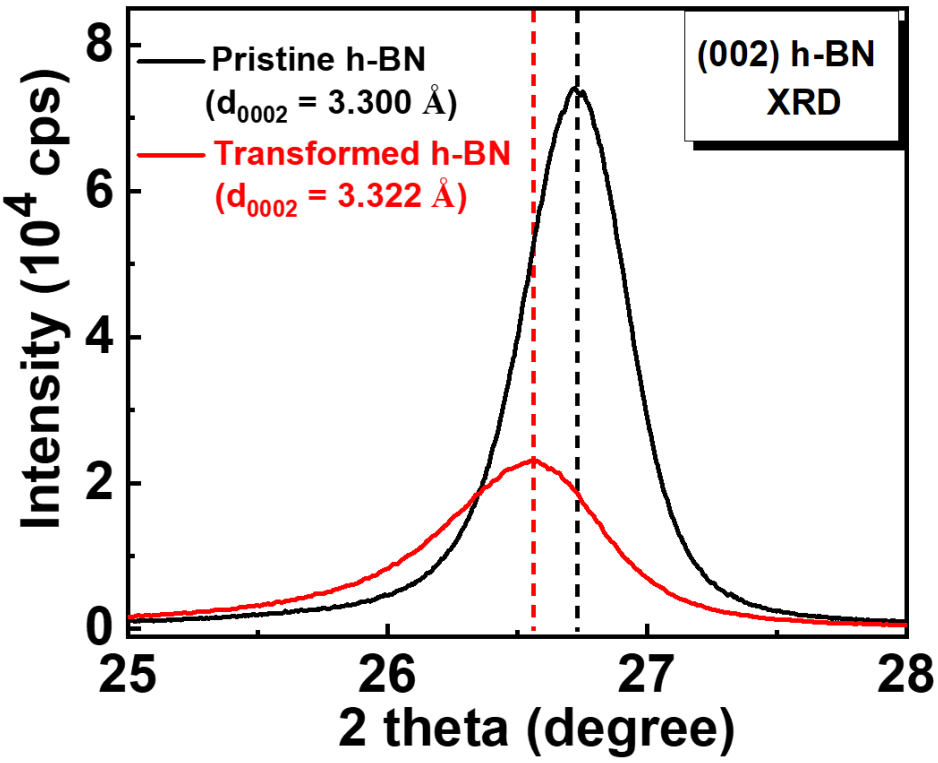

Figure S6. XRD comparison of pristine h-BN and transformed h-BN from c-BN (after the SPS). Comparison of (002) peak shows increased inter-planar *d* spacing after the SPS.

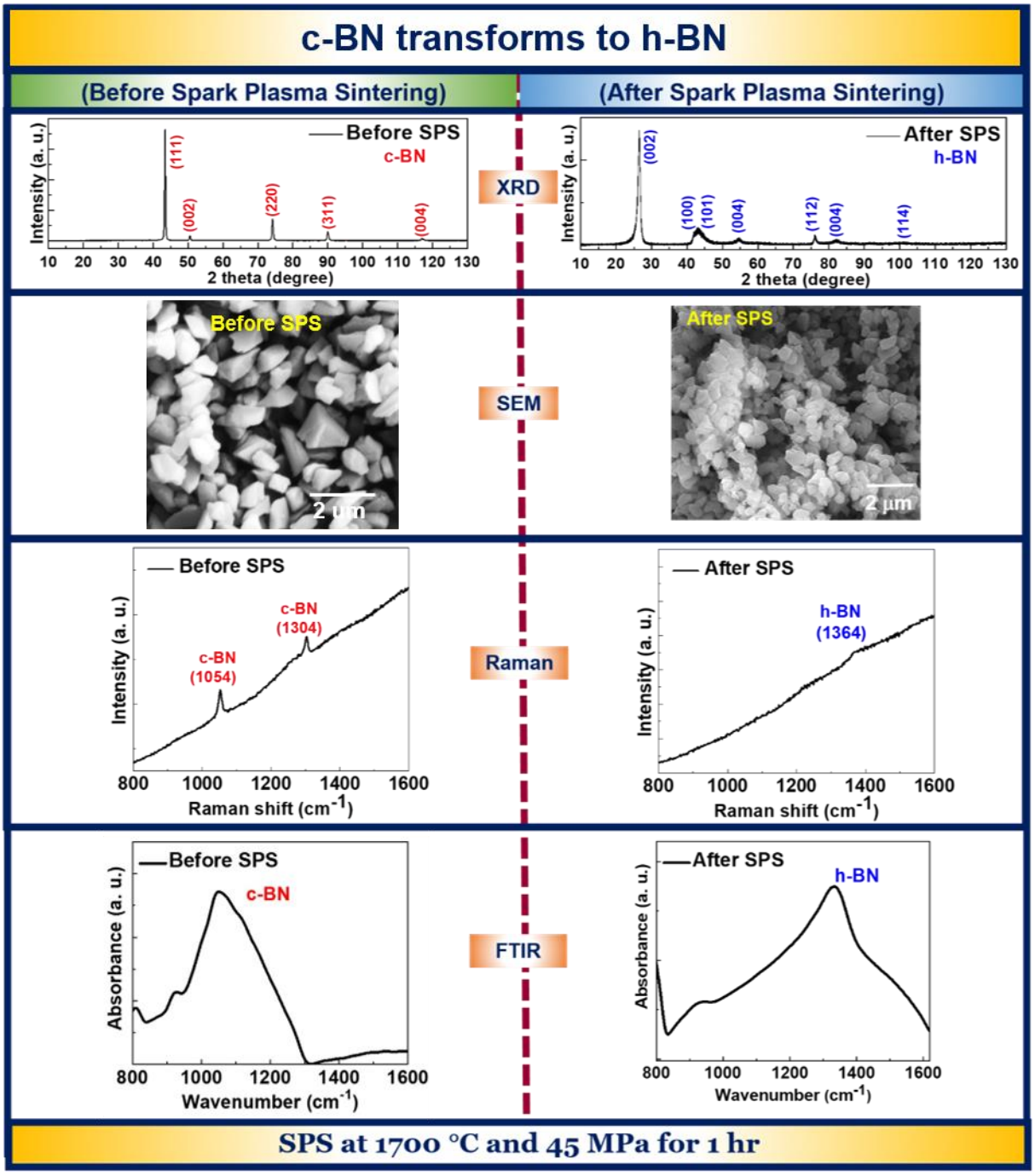

Figure S7. Characterizations of c-BN, before (left panel) and after the SPS (right panel). XRD, FESEM, Raman spectroscopy, and FTIR show that c-BN transforms to h-BN, after the SPS at 1700 °C and 45 MPa pressure.

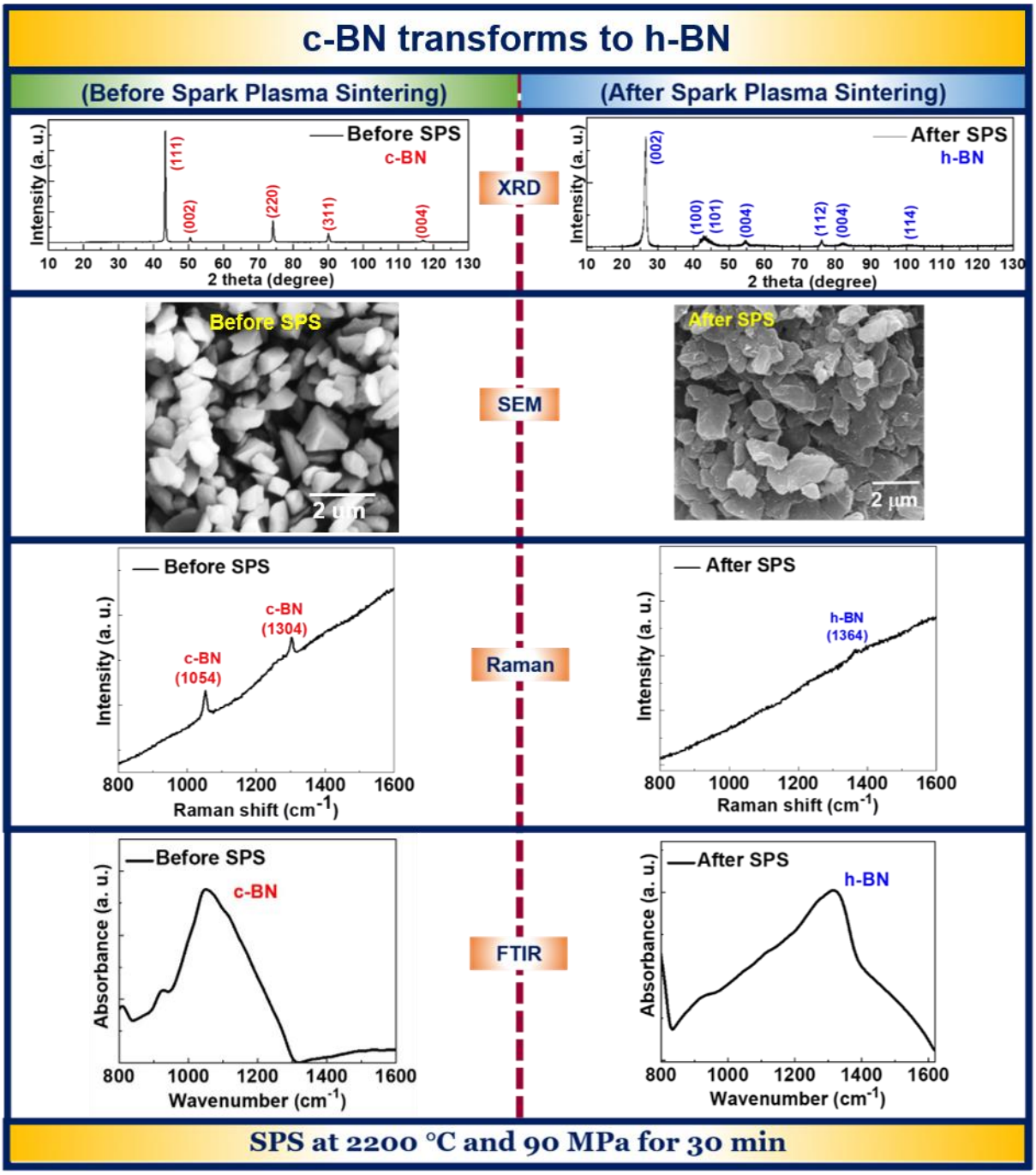

Figure S8. Characterizations of c-BN before (left panel) and after the SPS (right panel). XRD, FESEM, Raman spectroscopy, and FTIR shows that c-BN transforms to h-BN, after the SPS at 2200 °C and 90 MPa pressure. Due to experimental limitations at high temperature (2200 °C), SPS was performed for only 30 min.

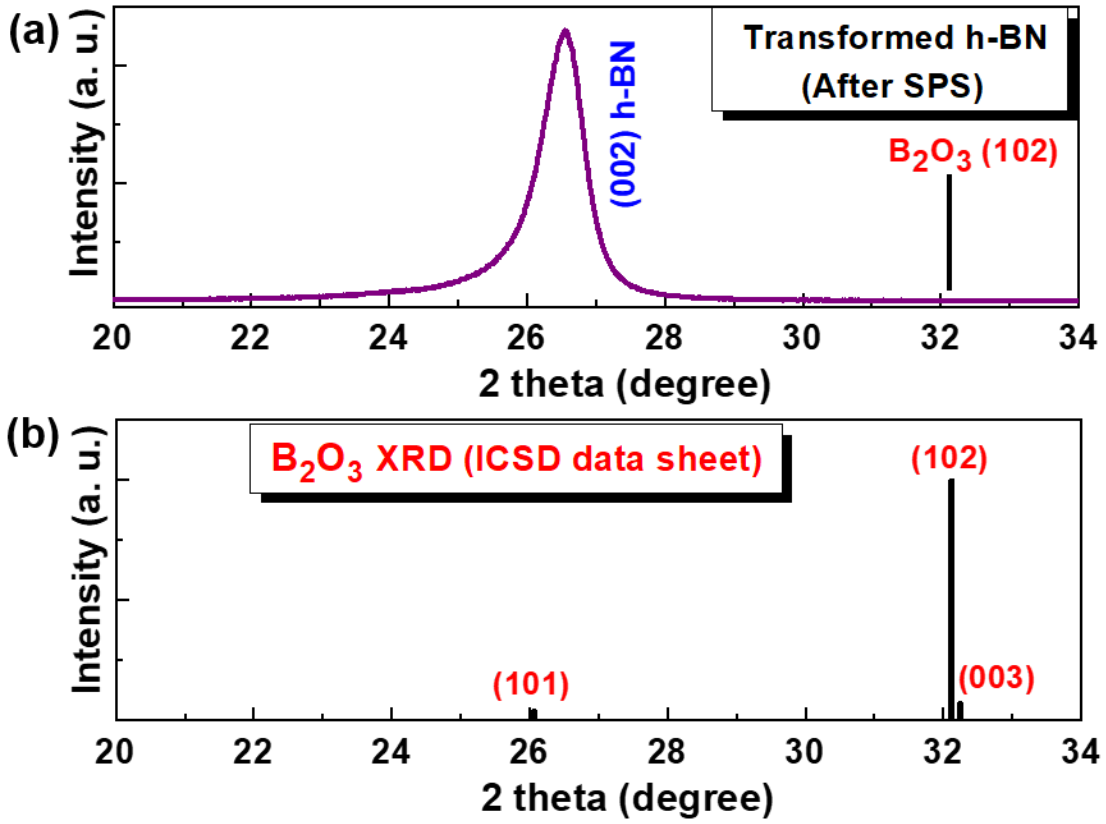

Figure S9. Search for B_2O_3 impurity peak. (a) XRD to search for the boron oxide (B_2O_3)-related impurity peaks, in transformed h-BN (after SPS of c-BN at 1700 °C, 90 MPa for 1 h). (b) XRD of B_2O_3 taken from the Inorganic Crystal Structure Database (ICSD - FIZ Karlsruhe, ID: 4561) with the strongest intense (102) peak at ~32.12°. As shown, we have not seen any peak at this position, confirming the absence of B_2O_3-related impurities in h-BN.

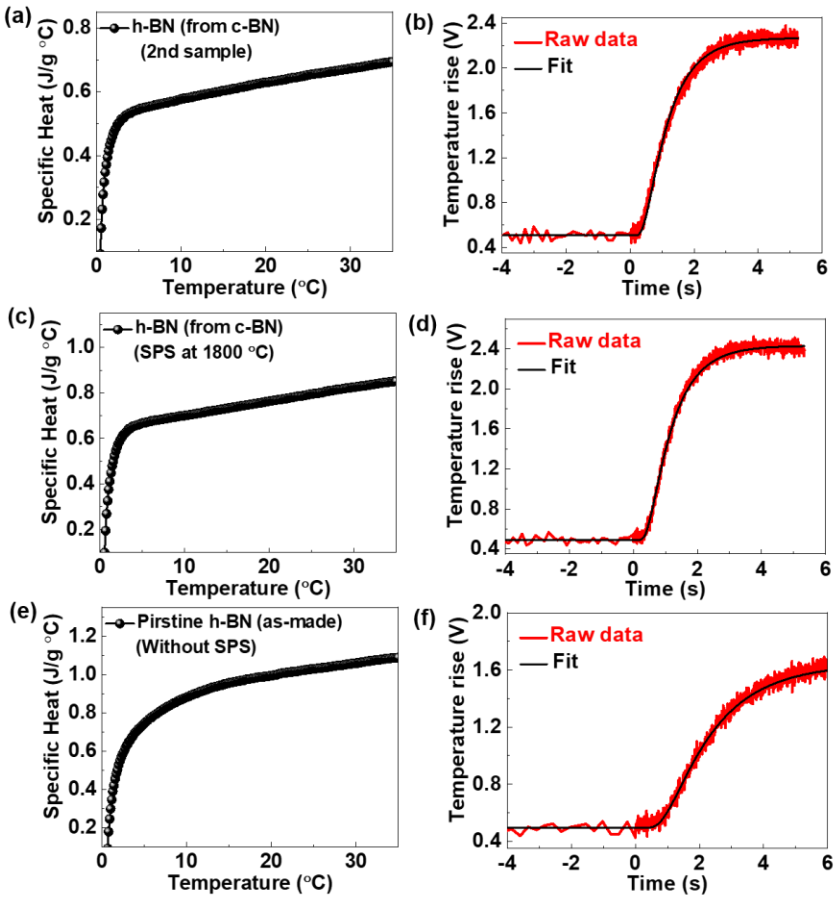

h-BN disk (Transformed from c-BN)	C_p (J/kg-K)	ρ (kg/m^3)	α (m^2/s)	k (W/mK)
SPS @ 1700 °C (Sample-1)	678	1784.07	2.72×10^{-06}	3.29
SPS @ 1700 °C (Sample-2)	628	1944.50	2.57×10^{-06}	3.13
SPS @ 1800 °C	761.5	1899.65	2.25×10^{-06}	3.26
Pristine h-BN (Without SPS)	915	1354.29	4.17×10^{-06}	5.17

Figure S10. Specific heat capacity (left panel) and laser flash method data (right panel) of phase transformed h-BN. (a) and (b) SPS of c-BN at 1700 °C (sample-2 for reproducibility). (c) and (d) SPS at 1800 °C (highest achievable temperature during SPS to make one-inch diameter disk). (e) and (f) pristine h-BN without SPS (for comparison). Our thermal conductivity measurement set up requires 1-inch (25 mm) diameter disk. For 2200 °C SPS case, we can only make disk of diameter 20 mm, not suitable for the thermal conductivity measurement.

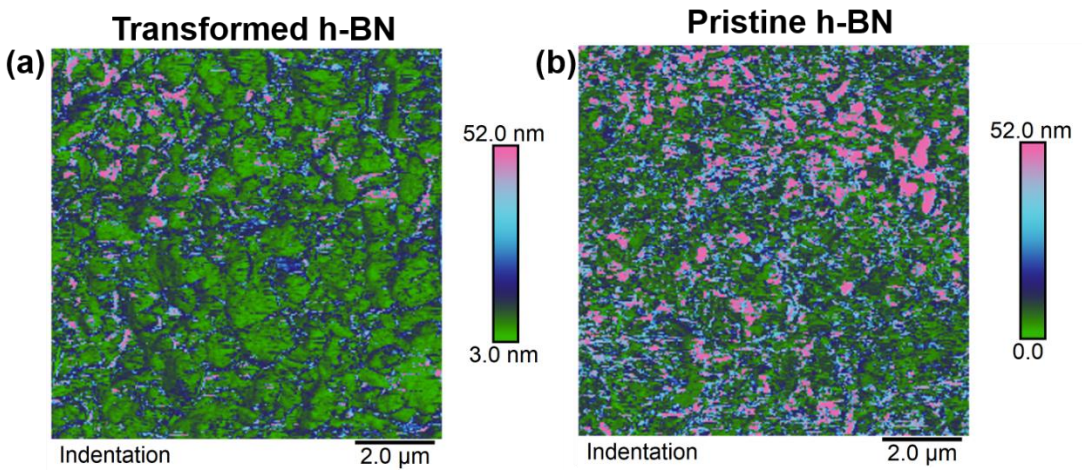

Figure S11. Elastic indentation depth map of (a) Transformed h-BN (from c-BN after the SPS) and (b) pristine as made h-BN (without SPS), carried out at fixed normal load (400 nN). The higher indentation depth reveals local sites of elastically softer regions observed in the pristine. No plastic deformation has been observed in this range of indentation depth.